High-speed droplet migration in silicon

H. E. Cline and T. R. Anthony

General Electric Research and Development Center, Schenectady, New York 12301
(Received 27 August 1975; in final form 6 February 1976)

High-temperature thermomigration of aluminum-rich droplets in silicon has resulted in droplet migration rates up to 10 cm/day. These unexpectedly high rates are an order of magnitude greater than those previously reported in the literature. The large enhancement of droplet migration rates at high temperatures is shown to be caused by a substantial increase in the flow of liquid across the droplet and by a favorable variation in the change of the composition of the liquid at high temperatures. The variation of droplet velocity with droplet size is reported over a large range of droplet sizes and temperatures for both the ⟨100⟩ and ⟨111⟩ migration directions in silicon. The undersaturation and supersaturation required to make a (111) silicon plane dissolve and deposit, respectively, are calculated from the data. Finally, from the velocity of large droplets, the liquid interdiffusion coefficient for the aluminum-silicon system is determined.

PACS numbers: 66.30.Kv, 81.20.Ily

I. INTRODUCTION

Liquid droplets in a solid migrate in a thermal gradient because atoms of the solid dissolve into the liquid at the hot interface of the droplet, diffuse across the droplet, and deposit on the cold interface of the droplet. The resulting flux of dissolved solid atoms from the hot to the cold side of the droplet causes the droplet to migrate towards the hot end of the crystal.

Previous experiments in a variety of materials[1–15] have shown droplet migration rates of less than 1 cm/day over a limited range of temperature. Since the transport of dissolved solid atoms across the droplet is limited ultimately by the magnitude of the liquid diffusion coefficient, high temperatures were not expected to markedly increase droplet migration rates because of the small temperature dependence of liquid diffusion coefficients. As a result, droplet migration experiments were never extended to relatively high temperatures.

However, as is shown in this paper, the equation for droplet migration must be modified at high temperatures to include both a variation in the change of composition of the droplet liquid with temperature and a physical flow of liquid that occurs across a droplet during migration. The resulting migration equation indicates a sharp increase in droplet migration rate at high temperatures. This prediction is confirmed experimentally in this paper by high-temperature droplet migration rates that are an order of magnitude greater than those previously reported in the literature.[15–33]

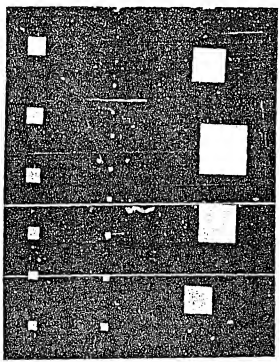

FIG. 1. The mask used to etch a series of square holes of varying size in a silicon wafer by photolithography techniques.

II. EXPERIMENTAL PROCEDURE

Two phosphorus-doped 10-Ω cm, silicon single crystals containing 10^4 dislocations/cm^2 and with respective ⟨100⟩ and ⟨111⟩ crystallographic orientations along their cylindrical axis were obtained from Texas Instruments Corp. From each 2.5-cm-diam by 40-cm-long crystal,

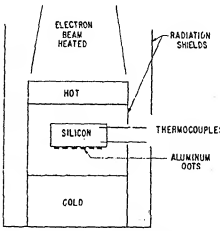

FIG. 2. The electron beam thermomigrates. The sample is suspended between a Mo block heated by an electron beam and a water-cooled copper block. The aluminum droplets previously deposited on the cooler face of the silicon wafer migrate up the temperature gradient through the wafer.

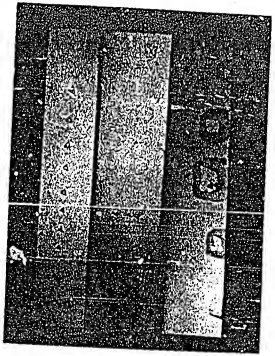

FIG. 3. The triangular cross section of doped trails left behind droplets migrating in the (111) direction as revealed by sectioning and staining. The larger droplets are unstable and are breaking up. 6× magnification.

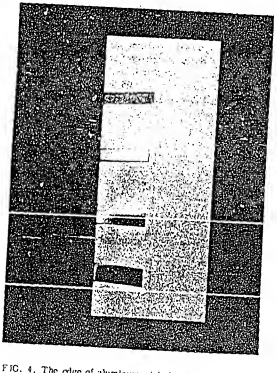

FIG. 4. The edge of aluminum-rich droplet migrating in the (111) direction in silicon in the form of a triangular platelet. Stained, 20×.

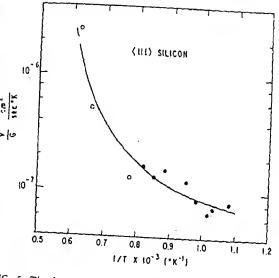

FIG. 5. The droplet velocity V of large droplets migrating in the (111) direction over the applied thermal gradient G versus the reciprocal of the absolute temperature.

a number of 1-cm-thick wafers were cut and polished to a 3-μ finish. Square holes, 30 μ of various sizes were etched in the silicon wafers using the mask shown in Fig. 1 and conventional photolithography techniques. An aluminum film 20 μ thick was deposited into the etched holes by electron beam evaporation from a Temescal Supersource in a vacuum of 10^{-6} Torr in 30 min. Following a 1-h anneal at 550 °C to ensure a strong bond between the aluminum film and the silicon, the excess aluminum between the etched holes was removed by mechanical polishing.

The sample was then placed in the radiation thermal gradient apparatus shown in Fig. 2 in a vacuum of 10^{-6} Torr. Both the temperature and the temperature gradi-

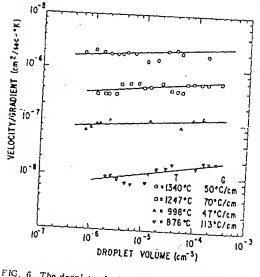

FIG. 6. The droplet velocity V of droplets migrating in the (111) direction over the applied thermal gradient G versus the volume of the droplets at various temperatures.

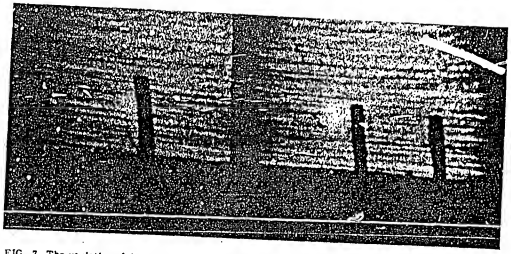

FIG. 7. The variation of droplet velocity with droplet size for droplets migrating in the (111) direction as revealed by the decrease in droplet penetration distance with decreasing droplet size in this infrared transmission photomicrograph 20 × magnification.

ent were recorded with Pt-10% Rh thermocouples inserted in holes in the side of the sample. After droplet migration, the wafers were sliced parallel to the row of droplets and the droplet migration distance was determined from infrared transmission microphotographs. Cross sections of the doped trails left behind the droplets were then revealed by sectioning and staining. In several cases, the shapes of the solidified droplet were examined in the scanning electron microscope after the surrounding silicon had been etched away with a solution of 10 HNO_3, 4 HAc, and 1 HF.

III. EXPERIMENTAL RESULTS

A. Migration in the (111) direction

In the (111) direction, an aluminum droplet migrates as triangular platelet laying in the (111) plane and bounded on its edges by (112) planes[7] (Figs. 3 and 4). Droplets larger than 0.10 cm on an edge are unstable[16,17] and break up into several droplets during migration (Fig. 3). Droplets smaller than 0.0175 cm did not migrate into the crystal because of a surface barrier problem.

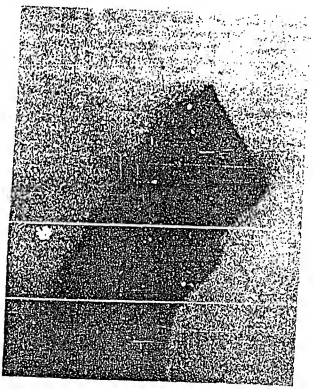

FIG. 8. An infrared transmission photomicrograph of a droplet pyramid migrating in the (100) direction as seen along the (110) direction. (175×.)

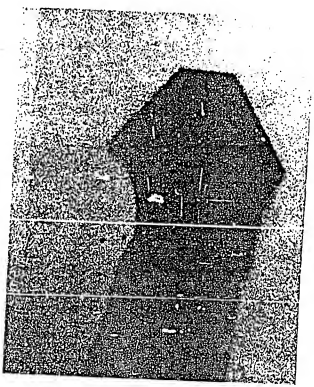

FIG. 9. A trapezoidal droplet migrating in the (100) direction as viewed in an infrared transmission photomicrograph along a (110) direction. (175×.)

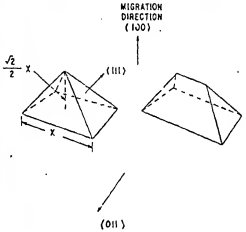

FIG. 10. A schematic diagram of how a regular pyramid droplet migrating in the (100) direction can distort into a trapezoidal droplet by the preferential dissolution of two opposing faces. (0.75×.)

The ratio of the droplet migration rate over the imposed thermal gradient is plotted in Fig. 5 as a function of temperature. At high temperatures, the droplet velocity increases rapidly with increasing temperature. The highest data point represents an actual measured velocity of 10 cm/day (1.2×10^{-4} cm/sec).

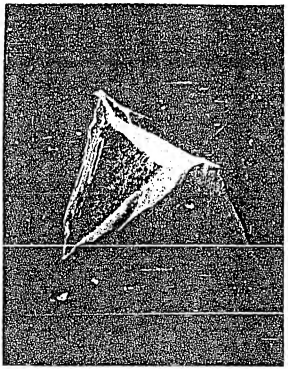

FIG. 11. A scanning electron micrograph of an aluminum-rich droplet migrating in the (100) direction with a pyramid shape. The silicon surrounding the droplet has been selectively etched away. An apparent 4-μ dissolution ledge appears along the upper left-hand edge of the droplets. (200×.)

FIG. 12. A scanning electron micrograph of kinks on the apparent dissolution ledge seen in Fig. 11. (5000×.)

The droplet migration rate is also affected by the droplet volume.[4,5,7,8] Figure 6 shows that the droplet migration rate decreases by a factor of 2 when the droplet volume is decreased by a factor of 200 in the Al-Si system. This decrease in droplet velocity with droplet size is apparent in the infrared transmission photograph of a row of droplets of varying size in Fig. 7.

B. Migration in the (100) direction

Aluminum-rich liquid droplets migrate in silicon in

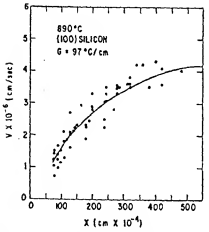

FIG. 13. The variation of the velocity of pyramid droplets migrating in the (100) direction versus the diameter of the base of the droplet pyramid, showing the decrease in droplet velocity with decreasing droplet size in the (100) direction.

the ⟨100⟩ direction as pyramids bounded by four forward ⟨111⟩ planes and a rear ⟨100⟩ plane (Fig. 8). The twisted doped trails left behind some droplets migrating in the ⟨100⟩ direction indicate that the four ⟨111⟩ facets do not always dissolve at a uniform rate. Nonuniform dissolution of the four forward ⟨111⟩ facets can also cause the regular pyramid shape of the droplet to become distorted into a trapezoid as shown experimentally in Fig. 9 and schematically in Fig. 10.

A scanning electron micrograph of a small droplet from which the surrounding silicon was selectively etched away is shown in Fig. 11. In this droplet, a 4-μ-deep ledge was seen on a dissolving ⟨111⟩ facet. At higher magnifications, kinks are observed on the ledge (Fig. 12). Evidence of such large dissolution ledges is also seen in infrared transmission of another droplet in Fig. 8.

Like the ⟨111⟩ direction, the droplet migration rate along the ⟨100⟩ direction also decreases with decreasing droplet size (Fig. 13). A comparison of Fig. 13 with Fig. 6 indicates that the decrease in droplet velocity with decreasing size in the ⟨100⟩ direction is twice that in the ⟨111⟩ direction.

IV. DISCUSSION

A. Effect of the temperature on the migration rate

To explain the marked increase in droplet velocity at high temperatures, a migration rate equation must be derived to include the effects of the mass flow of fluid across a droplet during migration and the variation in the change of composition of the liquid with temperature. Since the latter factor can be included in a straightforward way, let us concentrate for a moment on the effects of fluid flow across the droplet.

We consider the case of a binary droplet migrating in a thermal gradient in a solid (aluminum-rich liquid droplet in silicon) where one component (aluminum in our experiment) has a negligibly small solid solubility in the solid. A coordinate system moving with the droplet at the droplet velocity V is chosen for convenience since the droplet interfaces are stationary in this frame of reference. Conservation of mass of component 1 (silicon) at the rear interface of the droplet requires that the flux J_1 of component 1 passing across the droplet be equal to the removal rate VC_1^s of component 1 at the rear interface of the droplet.

$$J_1 = VC_1^s. \tag{1}$$

Here C_1^s is the concentration of component 1 in the solid phase. A similar mass conservation equation $J_2 = VC_2^s$ holds for component 2 (aluminum). However, since we are assuming that the solubility of component 2 is negligible (Al in solid Si) in the solid, the mass conservation equation for component 2 reduces to

$$J_2 = 0 \tag{2}$$

in the frame of reference of the moving droplet. That is, all of component 2 is carried along with the migrating droplet.

At first glance, the lack of a flux of component 2 is a little bit surprising since we know that a concentration gradient of component 1 *and* thus of component 2 is imposed across the droplet by the temperature gradient. Consequently, we would expect a diffusion flux of component 2 similar to the diffusion flux of component 1 which generates droplet migration. Although such a diffusion flux of component 2 does occur in the forward direction in the droplet, it is exactly canceled out by a flow or drift of the liquid[18–21] towards the rear interface of the droplet. If D_2 is the intrinsic diffusion coefficient of component 2 in the liquid and U^l is the drift velocity[18–21] of the liquid in the droplet, with respect to the moving interface, we can express this cancellation between the diffusion flux and fluid flow for component 2 as

$$J_2 = -D_2 \frac{\partial C_2^l}{\partial z} + U^l C_2^l = 0. \tag{3}$$

For component 1 on the other hand, the fluxes generated by the concentration gradient and the fluid flow are both towards the rear of the droplet and hence reinforce each other, causing the droplet to migrate more rapidly. This fluid flow U^l which increases with increasing temperature [because of the decrease of C_2^l with increasing temperature in Eq. (3)] is the direct cause of the marked increase in droplet migration rate at high temperatures. The total flux of component 1 in the droplet produced both by pure diffusion and fluid flow is

$$J_1 = -D_1 \frac{\partial C_1^l}{\partial z} + U^l C_1^l. \tag{4}$$

The two components of the liquid satisfy the relation

$$\bar{V}_1 C_1^l + \bar{V}_2 C_2^l = 1, \tag{5}$$

where $\bar{V}_1$ and $\bar{V}_2$ are respectively the partial molar volumes of components 1 and 2 in the liquid.

Combining Eq. (1)—(5) to eliminate J_1, J_2, $\partial C_1^l/\partial z$, and U^l, the velocity V of the migrating droplet is found to be

$$V = \frac{\bar{V}_1 C_1^l D_1 + \bar{V}_1 C_1^l D_2}{\bar{V}_2 C_2^l} \frac{\partial C_1^l}{\partial z}. \tag{6}$$

By using the definition of the interdiffusion coefficient $\tilde{D} = \bar{V}_2 C_2^l D_1 + \bar{V}_1 C_1^l D_2$, this expression simplifies to

$$V = \frac{\tilde{D}}{C_1^s \bar{V}_2 C_2^l} \frac{\partial C_1^l}{\partial z}. \tag{7}$$

At low temperatures in the Al-Si system where the droplet is largely liquid aluminum $C_2^l \bar{V}_2 \simeq 1$ and Eq. (7) reduces to

$$V = \frac{D_1}{C_1^s} \frac{\partial C_1^l}{\partial z}$$

which has been used previously to interpret liquid droplet migration in semiconductors.[5,6,12] Here D_1 is the intrinsic diffusion coefficient of Si in liquid aluminum, C_1^s is the number of moles/unit volume of silicon in solid silicon and $\partial C_1/\partial z$ is the concentration gradient of the silicon in the liquid aluminum droplet.

At high temperatures on the other hand, the phase

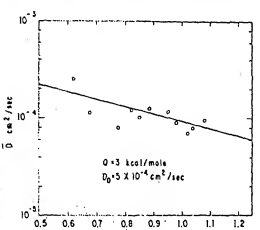

FIG. 14. The variation of the interdiffusion coefficient $\tilde{D}$ versus the reciprocal of the absolute temperature.

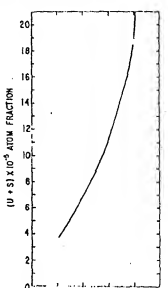

FIG. 15. The sum of the undersaturation U and supersaturation S required to cause respectively silicon dissolution and deposition on the forward and rear faces of a droplet migrating in the (100) direction at a rate appropriate to the droplet velocity V.

diagram of the Al-Si system causes the liquid droplet to be composed almost entirely of Si and $V_1^l C_1^l$ approaches unity, the velocity then becomes

$$V = \frac{D_s}{C_1^s C_1^l V_2^s} \frac{\partial C_1^l}{\partial z} ,$$

where D_s is the intrinsic diffusion coefficient of Al in liquid Si. Since $C_1^l \bar{V}_2^l \ll 1$, the droplet velocity becomes very large at high temperatures as we have observed. In the limit as $C_1^l \bar{V}_2^l \to 0$, the velocity of the droplet does not become infinite however, since our assumptions of uniform fluxes and neglect of the latent heat evolved and absorbed respectively on the depositing and dissolving interfaces breakdown at extremely large droplet velocities.

B. Interface kinetics and the interdiffusion coefficient

The composition gradient $\partial C_1^l/\partial z$ in the liquid droplet can be calculated by dividing the concentration drop ΔC_1^l across the droplet by the droplet thickness L ($\partial C_1^l/\partial z = \Delta C_1^l/L$). The concentration drop ΔC_1^l is generated by the change in solubility ($\partial C_E/\partial T)GL$ induced by the temperature change GL across the droplet minus the undersaturation U and supersaturation S required to cause dissolution and deposition on the forward and rear interfaces of the droplet [$\Delta C_1^l = |(\partial C_E/\partial T)GL - U + S|$].[4,5] Thus

$$\frac{\partial C_1^l}{\partial z} = \frac{\partial C_E}{\partial T} G - \frac{U+S}{L} . \qquad (8)$$

In the Al-Si system, the temperature gradient G in the droplet is equal to the applied thermal gradient because the thermal conductivities of the solid and liquid are nearly equal.[6,7]

TABLE I. The variation of the reciprocal of the atomic fraction of Al ($C_1^l \bar{V}_2^l$) and the slope of the equilibrium solubility of Si in the liquid droplet versus temperature. These factors alone predict increase in droplet migration rate of 40 times between 600 and 1400°C

T (°C)	$\frac{1}{C_1^l V_2^s}$	$\frac{\partial C_E}{\partial T} \times 10^4$	$\frac{1}{C_1^l V_2^s} \frac{\partial C_E}{\partial T} \times 10^4$
600	1.15	6.6	7
700	1.25	7.5	9
800	1.38	7.9	11
900	1.56	8.4	13
1000	1.78	8.8	16
1100	2.12	10.0	21
1200	2.78	12.1	33
1300	4.55	14.3	59
1400	16.65	16.6	278

1. The interdiffusion coefficient

At large droplet sizes we may neglect the interface kinetic term in Eq. 8. The droplet velocity from Eqs. (7) and (8) then becomes

$$V = \frac{\tilde{D}}{(C_2^s \bar{V}_2^l) C_2^s} \frac{\partial C_E}{\partial T} G \qquad (9)$$

which may be used to calculate the interdiffusion coefficient $\tilde{D}$ as shown in Fig. 14. With $D = D_0 \exp(-Q/RT)$, values of $D_0 = 5 \times 10^{-4}$ cm^2/sec and $Q = 3$ kcal/mole were obtained which are in close agreement with liquid diffusion coefficients measured by other techniques.[22,23] Since the interdiffusion coefficient depends only weakly on temperature, it is apparent that the large variation in the droplet migration rate with temperature (Fig. 5) is caused by the large changes of $1/C_1^l V_2^l$ and $\partial C_E/\partial T$ with temperature (see Table I).

2. Interface kinetics

From the variation of droplet velocity V with droplet thickness L [see Eqs. (7) and (8)], the undersaturation U and supersaturations S required respectively on the dissolving and depositing faces of the droplet can be calculated. For droplets migrating in the (100) direction,

$$U+S=50V_{100}\ \frac{\text{atom fractions}}{\text{cm/sec}}$$

where V_{100} is the velocity of the droplets in the ⟨100⟩ direction in cm/sec and $U+S$ is expressed in concentration units of atom fractions. Since both the pyramid droplets migrating along the ⟨100⟩ and the triangular platelets migrating along the ⟨111⟩ have {111} facets for their forward and rear faces, one would expect that the $U+S$ values, after a correction for the effective thickness L of the pyramid droplet and the resolved normal velocity of its {111} facets, would be equal. In fact, both the ⟨100⟩ data and the {111} data indicate that $U+S$ (111 facets) $=200V_{111}$ (atom fraction) $(\text{cm/sec})^{-1}$, where V_{111} is the normal resolved velocity of a 111 facet plane in cm/sec.

C. Migration velocity

A more useful expression for the migration velocity may be derived in terms of atomic fraction X of the droplet element (in our case aluminum). The equilibrium composition of the liquid is given on a phase diagram of the system of interest. We convert our expression (9) to atomic fraction using the relations $C_1V_1=X$ and $C_2V_2=1-X$. We approximate $(1/C_2')(\partial C_E/\partial T)$ by the liquidus slope $\partial X/\partial T$ because volume changes are usually small. We obtain an expression for the velocity

$$V=\frac{D}{1-X}\left(\frac{\partial X}{\partial T}\right)G \tag{10}$$

that clearly shows the effect of enchanced velocity as $X\to 1$ which occurs at high temperatures. The diffusivity of most liquids are similar and do not vary much with temperature. Also the value of the thermal gradient in the solid is not expected to vary much for a given apparatus. Thus the main factor determining the migration velocity is the solubility in the liquid as a function of temperature.

Doping semiconductors to produce electronic devices[24–32] may be done much more rapidly by droplet migration than by conventional solid-state diffusion. A significant amount of time may be saved by using high temperatures to obtain high migration velocities.

[1] W. A. Whitman, Am. J. Sci. XI, 126 (1926).
[2] W.D. Kingery and W.H. Goodnow, *Glaciology Ice, Snow, Properties, Processes and Applications*, edited by W.D. Kingery (MIT Press, Cambridge, Mass., 1963), p. 237.
[3] D. Hoekstra, T.E. Osterkamp, and W.F. Weeks, J. Geophys. Res. 70, 5035 (1965).
[4] T.R. Anthony and H.E. Cline, J. Appl. Phys. 42, 3380 (1971).
[5] H.E. Cline and T.R. Anthony, J. Appl. Phys. 43, 10 (1972).
[6] T.R. Anthony and H.E. Cline, J. Appl. Phys. 43, 2473 (1972).
[7] H.E. Cline and T.R. Anthony, J. Appl. Phys. 43, 4391 (1972).
[8] T.R. Anthony and H.E. Cline, Acta Met. 20, 247 (1972).
[9] T.R. Anthony and H.E. Cline, Philos. Mag. 22, 893 (1970).
[10] D.R.H. Jones and G.A. Chadwick, Philos. Mag. 24, 1327 (1971).
[11] R.L. Bradshaw and F. Sanchez, J. Geophys. Res. 74, 4209 (1969).
[12] V.N. Lozovskii and A.I. Udyanskaya, Sov. Phys.-Crystallogr. 13, 477 (1968).
[13] W.R. Wilcox and P.J. Schlicta, J. Appl. Phys. 42, 1823 (1971).
[14] W.R. Wilcox, Ind. Eng. Chem. 60, 13 (1968).
[15] W.R. Wilcox, Ind. Eng. Chem. 61, 76 (1969).
[16] T.R. Anthony and H.E. Cline, Acta Met. (to be published).
[17] H.E. Cline and T.R. Anthony, Acta Met. (to be published).
[18] G.S. Hartley and J. Crank, Trans. Faraday Soc. 45, 801 (1949).
[19] R.M. Barrer, J. Phys. Chem. 61, 178 (1957).
[20] V. Freise, J. Chem. Phys. 57, 879 (1957).
[21] A.W. Adamson and R. Irani, J. Chem. Phys. 55, 102 (1958).
[22] N.H. Nachtrieb, Adv. Phys. 16, 309 (1967).
[23] Y.P. Gupta, Adv. Phys. 16, 333 (1967).
[24] W.G. Pfann, U.S. Patent 2,770,761 (1956).
[25] W.G. Pfann, U.S. Patent 2,813,048 (1957).
[26] T.R. Anthony and H.E. Cline, U.S. Patent 3,900,736 (1975).
[27] H.E. Cline and T.R. Anthony, U.S. Patent 3,899,362 (1957).
[28] T.R. Anthony and H.E. Cline, U.S. Patent 3,895,967 (1975).
[29] H.E. Cline and T.R. Anthony, U.S. Patent 3,899,361 (1975).
[30] T.R. Anthony and H.E. Cline, U.S. Patent 3,904,442 (1975).
[31] H.E. Cline and T.R. Anthony, U.S. Patent 3,898,106 (1975).
[32] T.R. Anthony and H.E. Cline, U.S. Patent 3,902,925 (1975).

Vol. 47 1976